frontiers in Chemistry

ORIGINAL RESEARCH
published: 03 December 2021
doi: 10.3389/fchem.2021.786367

Synthetic Strategy Towards Heterodimetallic Half-Sandwich Complexes Based on a Symmetric Ditopic Ligand

*Lewis P. M. Green[1], Tasha R. Steel[1], Mie Riisom[1,2], Muhammad Hanif[1], Tilo Söhnel[1], Stephen M. F. Jamieson[2], L. James Wright[1], James D. Crowley[3] and Christian G. Hartinger[1]**

[1]School of Chemical Sciences, University of Auckland, Auckland, New Zealand, [2]Auckland Cancer Society Research Centre, University of Auckland, Auckland, New Zealand, [3]Department of Chemistry, University of Otago, Dunedin, New Zealand

Multimetallic complexes have been shown in several examples to possess greater anticancer activity than their monometallic counterparts. The increased activity has been attributed to altered modes of action. We herein report the synthesis of a series of heterodimetallic compounds based on a ditopic ligand featuring 2-pyridylimine chelating motifs and organometallic half-sandwich moieties. The complexes were characterized by a combination of ^{1}H NMR spectroscopy, electrospray ionization mass spectrometry, elemental analysis and single crystal X-ray diffraction. Investigations into the stability of representative complexes in DMSO-d_6 and 10% DMSO-d_6/D_2O revealed the occurrence of solvent-chlorido ligand exchange. Proliferation assays in four human cancer cell lines showed that the Os-Rh complex possessed minimal activity, while all other complexes were inactive.

Keywords: anticancer activity, structural characterization, ligand exchange reactions, bioorganometallics, heterodimetallic complexes

OPEN ACCESS

Edited by:
Dinorah Gambino, Universidad de la República, Uruguay

Reviewed by:
Alzir Azevedo Batista, Federal University of São Carlos, Brazil
Roberto Santana Da Silva, University of São Paulo, Brazil

****Correspondence:***
Christian G. Hartinger
c.hartinger@auckland.ac.nz

Specialty section:
This article was submitted to Medicinal and Pharmaceutical Chemistry, a section of the journal Frontiers in Chemistry

Received: *30 September 2021*
Accepted: *02 November 2021*
Published: *03 December 2021*

Citation:
Green LPM, Steel TR, Riisom M, Hanif M, Söhnel T, Jamieson SMF, Wright LJ, Crowley JD and Hartinger CG (2021) Synthetic Strategy Towards Heterodimetallic Half-Sandwich Complexes Based on a Symmetric Ditopic Ligand. Front. Chem. 9:786367. doi: 10.3389/fchem.2021.786367

1 INTRODUCTION

Metals play various roles in biological processes (Buccella et al., 2019), e.g., proteins often use metal centers to adopt certain structures or as catalytically active sites (Haas and Franz, 2009; Wodrich and Hu, 2017; Ghosh et al., 2021). Metal complexes, most often platinum compounds, have been used for a long time to treat cancer (Jakupec et al., 2008; Kenny and Marmion, 2019; Simpson et al., 2019; Boros et al., 2020; Tremlett et al., 2021). In addition to the clinically successful DNA-targeting cis-, carbo- and oxaliplatin (Johnstone et al., 2014), other mononuclear species studied include Ru, Os, Rh and Ir-based compounds (Sava et al., 2003; Arango et al., 2004; Hartinger et al., 2008; Geldmacher et al., 2012; Maillet et al., 2013). The non-Pt complexes have been headlined by various Ru-based examples, including the clinically explored KP1339 (Jakupec et al., 2008; Heffeter et al., 2010).

Synthetic attempts to link one or more metal-containing fragments have been made in order to obtain compounds with higher potency and modes of action different from those of the established anticancer agents. The tris-Pt compound BBR3464 (**Figure 1**) features Pt centers which contribute to DNA binding through electrostatic or covalent interactions (Manzotti et al., 2000). Indeed, the DNA binding of BBR3464 was found to be considerably different to that of cisplatin and the compound was found to show no cross-resistance in cancer cells (Manzotti et al., 2000; Ruhayel et al., 2012). Inspired by this approach, we reported organometallic compounds containing two metal centers coordinated to a maltol-derived bis(3-hydroxy-2-methyl-4-pyridone) ligand bridged by a spacer of

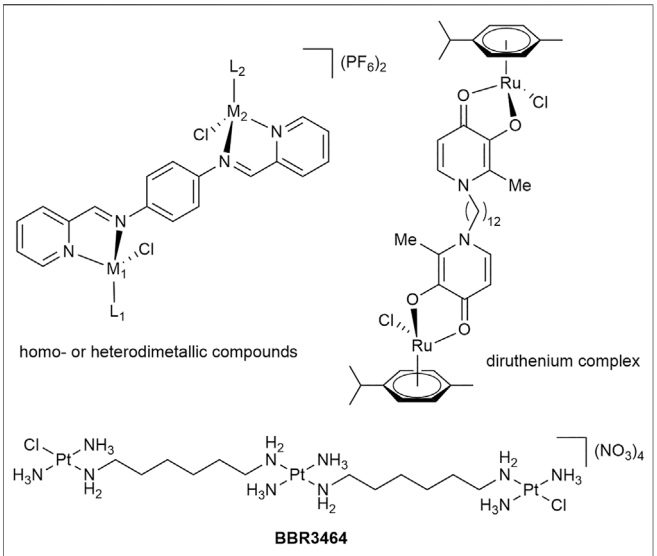

FIGURE 1 | Homo- and heterometallic complexes with anticancer activity.

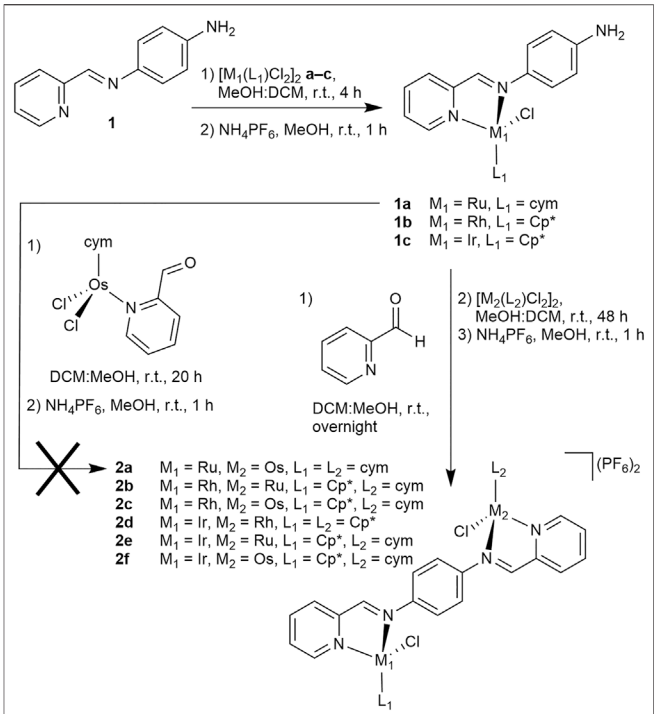

SCHEME 1 | Synthetic strategy towards heterodimetallic complexes **2a**–**2f**.

varying length (**Figure 1**) (Mendoza-Ferri et al., 2008; Parveen et al., 2019b). The IC_{50} value for the dodecane-bridged bis-Ru complex in SW480 cancer cells was similar to that of platinum reference compounds and was an order of magnitude lower than of the clinically-studied Ru(III) compound KP1019 (Mendoza-Ferri et al., 2008; Mendoza-Ferri et al., 2009; Nováková et al., 2009; Nazarov et al., 2018), while the mononuclear analog gave IC_{50} values greater than 100 μM, indicating a lack of cytotoxic activity (Mendoza-Ferri et al., 2008). Multimetallic triruthenium-carbonyl clusters (Gonchar et al., 2020) have also been found to be cytotoxic, and the most active of these clusters was shown to be a system that featured a glucose-inspired phosphorus ligand. The IC_{50} values for the clusters were in the sub-μM range for wildtype and cisplatin-resistant human ovarian cancer cells (Gonchar et al., 2020). Further to this triruthenium cluster, we have investigated the use of easily synthesized ditopic ligands to form homodimetallic complexes (**Figure 1**, top left). These structures were important as they highlighted the possibility for the rapid formation of a range of homo- and heterodimetallic species. Although the compounds had poor cytotoxicity in comparison to other dimetallic compounds (Steel et al., 2021), synthetic alterations to the ditopic ligand being used could easily yield more potent metal-based chemotherapeutics. Alternatively, scaffold structures can be adopted to form dimetallic species of greater complexity. Relevant examples include a trimeric scaffold consisting of alkylated 1,3,5-triaza-7-phosphaadamantane moieties or other phosphine or nitrogen donor-based ligand systems (Burgoyne et al., 2016; Batchelor et al., 2019; Curado et al., 2019). Moreover, tetra- and octanuclear Ir and Rh complexes can be created using dendritic structures that have Schiff-base ligands based on poly(propyleneimine) scaffolds (Payne et al., 2013). These metallodendrimers highlight an interesting trend whereby increasing multinuclearity resulted in an analogous increase in cytotoxicity as compared to the mono-metallic derivatives (Payne et al., 2013).

The nature of the anticancer activity observed for multimetallic compounds is likely to be different from those found for the corresponding monometallic analogs due to altered molecular modes of action, as discussed above for BBR3464 and closely related compounds (Ruhayel et al., 2012). Besides DNA, bis- and tris-Pt complexes can also bind to proteoglycans through sulfate anchoring (Gorle et al., 2018; Gorle et al., 2021). The resulting metalloshielding stops enzyme degradation and has recently been shown to be biologically relevant in cells (Gorle et al., 2018; Gorle et al., 2021). This method of template protection, a strategy analogous to complex–DNA binding, heralds a new avenue in the mechanisms of action for multimetallic compounds (Gorle et al., 2021).

Recent investigations have also demonstrated that cytotoxic efficacy can be altered when heterodimetallic systems are employed or could be used to release cytotoxic payload (Herry et al., 2019; Jain, 2019; Lisboa et al., 2020; Lisboa et al., 2021). The distinct properties of each metal center in terms of inertness, redox properties and affinity to bioligands will determine the lipophilic character and biological target binding ability of heterometallic compounds (Benjamin Garbutcheon-Singh et al., 2011; Parveen et al., 2019a; Batchelor et al., 2019). Mixing and matching these characteristics within one compound carves out new chemical space in the development of chemotherapeutic agents. For example, a Fe-Ru phosphane-bridged complex in ovarian carcinoma cell lines showed increased activity over the Ru-Ru analogue (Herry et al.,

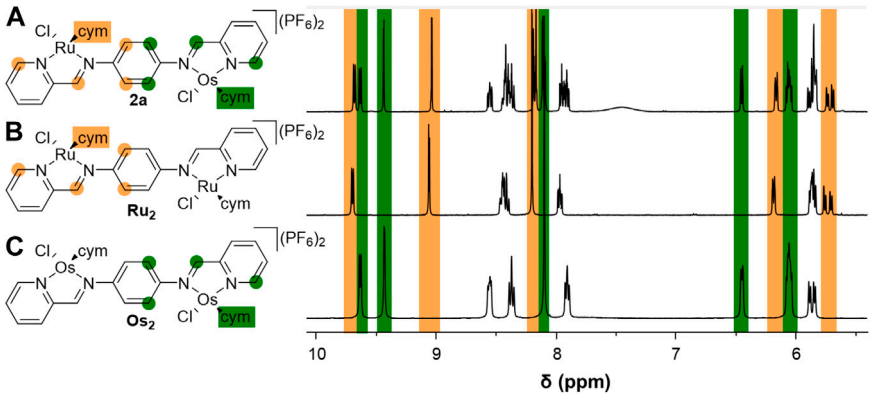

FIGURE 2 | Comparison of the ^{1}H NMR spectra for the heterodimetallic Ru-Os complex **2a (A)**, to those of the symmetric **Ru_2 (B)** and **Os_2 (C)** derivatives.

2019). The difference in activity was hypothesized to be the result of the Fe center facilitating the cellular uptake of the compound (Herry et al., 2019). Heteronuclear transition metal systems have also been investigated as theranostics (Redrado et al., 2021), in which the therapeutic can be traced *via* the diagnostic component of the molecule. Most often in theranostics, a fluorophore is conjugated to the metal-based therapeutic, for example, as in the recently reported gold- and ruthenium-based complexes with therapeutic and imaging capability (Bertrand et al., 2016). Polyaryl derivates like anthracene or pyrene are common fluorophores in theranostics, as is BODIPY (Bertrand et al., 2018). The versatility of BODIPY has allowed it to be incorporated into Pt-, Au-, Ru-, Ti- and Ir-based therapeutics (Bertrand et al., 2018). The formation of dimetallic theranostic compounds is also possible, yet slightly more complex (Bertrand et al., 2016). Two recent examples have paired tris(bipyridine) ruthenium and a Ru–porphyrin with therapeutics developed around a Au center (Bertrand et al., 2016). The range of investigations that have been conducted into the creation and use of heterodimetallic systems has highlighted the myriad of potential advantages afforded by employing compounds with different metal centers.

Herein, we report the synthesis and characterization of heterodimetallic complexes based on a symmetric ditopic 2-pyridylimine ligand. The stabilities of these complexes in DMSO and aqueous solutions were investigated and the cytotoxicities of the complexes in human cancer cells were determined.

2 RESULTS AND DISCUSSION

Recently, we reported the preparation of homodimetallic compounds of a symmetric, ditopic 2-pyridylimine-based ligand featuring a 1,4-diaminobenzene spacer (**Figure 1**, L_{DAB}), which is known to form stable coordination complexes (Steel et al., 2021). The formation of these di-Ru, -Os, -Rh and -Ir compounds with two different ditopic ligands highlighted the ability to reliably obtain

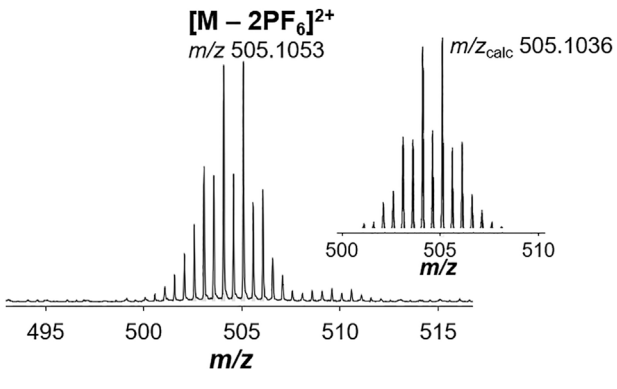

FIGURE 3 | ESI-mass spectrometry data for the Os-Ir complex **2f** compared to the calculated isotope pattern for the $[M - 2PF_6]^{2+}$ cation.

homodimetallic compounds in good yield (Steel et al., 2021). The complexes also demonstrated a range of structural characteristics and cytotoxic activity (Steel et al., 2021). In the case of those homodimetallic complexes, the ligand was prepared before it was decorated with metal centers. This was feasible due to the symmetric nature of the target complexes. To prepare low-symmetry heterodimetallic compounds based on the same ligand the synthetic strategy had to be adapted, as the previously reported route would likely lead to a mixture of compounds. Accordingly, different pathways were explored (**Scheme 1**). Initially, inspired by our recent work generating heterometallic PdPt caged systems (Lisboa et al., 2020), we investigated a two-step process, in which the mononuclear precursor **1a** would be formed by reaction from mono-topic 2-pyridylimine ligand **1** with dimeric $[Ru(cym)Cl_2]_2$ **a** (cym = η^6-*p*-cymene), followed by conversion with the preformed second metal fragment [Os(cym)(2-pyridine carboxaldehyde)Cl_2]$_2$ to target compound **2a**. Indeed, **1a** was prepared in very good yield (92%), however, the subsequent reaction with [Os(cym)(2-pyridine carboxaldehyde)Cl_2]$_2$ only provided **2a** in trace amounts

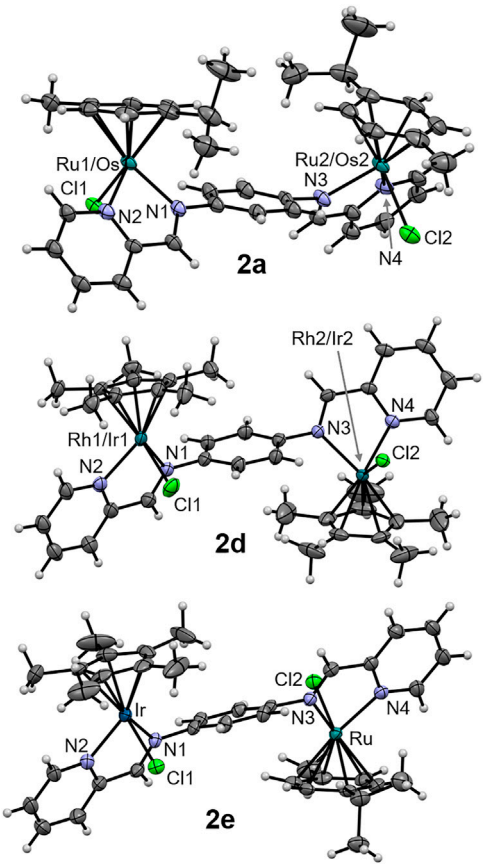

FIGURE 4 | ORTEP representation of one of the two enantiomers of complexes **2a**, **2d** and **2e** drawn at 50% probability level. Any co-crystallized solvent molecules and hexafluorophosphate counterions have been omitted for clarity.

(**Scheme 1**). In an alternative approach, **1a** was first treated with 2-pyridine carboxaldehyde to generate the second 2-pyridylimine binding site *in situ*, and the subsequent reaction with $[Os(cym)Cl_2]_2$ afforded **2a** in excellent yield (84%).

In the ^{1}H NMR spectrum of complex **2a** peaks characteristic of π-coordinated cym were observed, with the expected integrals relative to the ligand proton signals. Notably, in contrast to the symmetric dimetallic complexes (**Ru**$_2$ and **Os**$_2$, **Figure 2**), the phenylene protons resonated as two distinct doublets due to the lower molecular symmetry, whereas the corresponding protons in the higher symmetry **Ru**$_2$ and **Os**$_2$ complexes were singlets (Steel et al., 2021). The incorporation of two different metals and the resulting loss of symmetry within the molecule also resulted in more complex sets of signals for the remaining protons (**Figure 2** and **Supplementary Figure S19**). For example, the ^{1}H NMR spectrum of **2a** features two sets of resonances for the α-pyridyl and imine protons of the coordinating 2-pyridylimine units (**Figure 2**). The chemical shift values for one set of the α-pyridyl and imine resonances match well with those observed for the homodimetallic **Ru**$_2$, whilst the second set of peaks display chemical shift values that are very similar to those observed in the **Os**$_2$ complexes (**Figure 2**). These data are consistent with the presence of two distinct 2-pyridylimine units in **2a**, one coordinated to a [Ru(cym)Cl] fragment and the second binding to an [Os(cym)Cl] unit. In the electrospray ionization (ESI) mass spectrum of **2a**, the pseudomolecular ion $[M - 2PF_6]^{2+}$ was observed as the base peak at *m/z* 459.0743 (m/z_{calc} 459.0710; **Supplementary Table S1**) with the isotope pattern matching that predicted for the heterodimetallic complex, in addition to $[M - PF_6]^+$ at *m/z* 1,063.1156 (m/z_{calc} 1,063.1067).

The heterodimetallic compounds **2b**–**2f** were also synthesized in good yields (**Scheme 1**; 42–67%) from the mononuclear precursors **1b** (for **2b** and **2c**) and **1c** (for **2d**–**2f**) using the same strategy as for **2a** and the purity was confirmed by elemental analysis. We considered the relative labilities of the metal centers in the synthetic strategy to optimize the purity, as substitution of the metal center may occur *in situ* and result in the formation of undesired homodimetallic species. To mitigate the possibility of this occurring, the relatively inert Ir precursor **1c** was selected for use in the first reaction step when preparing **2d**–**2f**. ^{1}H NMR spectra of **2b**–**2f** were all indicative of formation of the heterodimetallic complexes (**Supplementary Figure S19**). By comparison with the equivalent homodimetallic complexes, in particular the protons adjacent to the pyridine and imine nitrogen atoms shifted characteristically depending on the nature of the metal center. ESI-mass spectrometry (MS) was used to characterize the complexes further and the mass spectra of **2b** and **2d**–**2f** featured signals assignable to the $[M - PF_6]^+$ and $[M - 2PF_6]^{2+}$ pseudomolecular ions (**Supplementary Table S1**), with the latter usually being present in higher abundance. Each of these peaks showed clearly the isotope pattern expected for the heterodimetallic complex (compare **Figure 3** for **2f**). In addition to these ions, we often detected, and in particular for **2c**, some single imine hydrolysis of the ligand, resulting in the loss of a pyridyl fragment, one of the metal centers and the respective π-bound ligand moiety, giving peaks corresponding to the mononuclear species $[M - C_6H_5N - M(L)Cl - 2PF_6]^+$. It should be noted that usually we detected ions that could be assigned to both metal moieties of the heterodimetallic complexes.

The molecular structures of the complexes **2a**, **2d** and **2e** were determined by single crystal X-ray diffraction studies (**Figure 4**). The single crystals were grown *via* the slow diffusion of toluene into a saturated solution of the respective complex in acetonitrile. All complexes have a triclinic crystal system and crystallized in the *P*-1 space group. While **2a** co-crystallized with an acetonitrile molecule, the structure of **2d** featured a disordered toluene molecule which was found sandwiched between the Cp* ligands of two neighboring molecules of **2d** (**Figure 5A**). The molecular structure of **2e** also contains a strongly disordered toluene molecule, which was excluded from the final refinement (**Supplementary Figure S20**, **Supplementary Table S2**). The structure features a co-crystallized water molecule, resulting in hydrogen bonding with the chlorido ligand coordinated to the Ru center, [d(Cl2–O) = 3.205 Å], and one of the PF_6^- counterions (d(F10–O) = 2.929 Å). Furthermore, in all three structures, the PF_6^- counterions were extensively involved in H bonding networks with several neighboring complex molecules (**Figure 5B** for that of **2a**). In the cases of **2a** (with cym

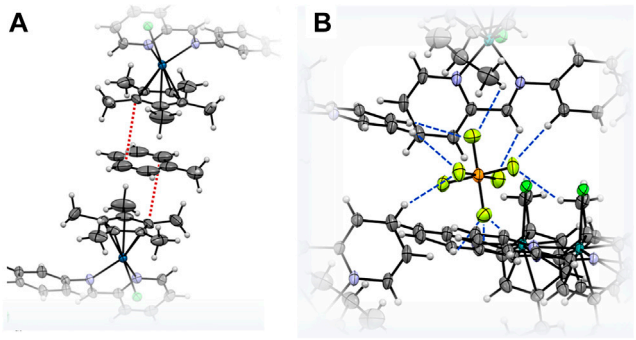

FIGURE 5 | ORTEP representation of **(A)** co-crystallized toluene π-bonding with the Cp* ligands of two adjacent molecules of **2d**, and **(B)** H-bonding network around a PF_6^- counteranion and **2a** molecules. The shortest C–C distances at 3.604 Å in **(A)** are highlighted by red dashed lines while the H bonds in **(B)** are indicated in blue.

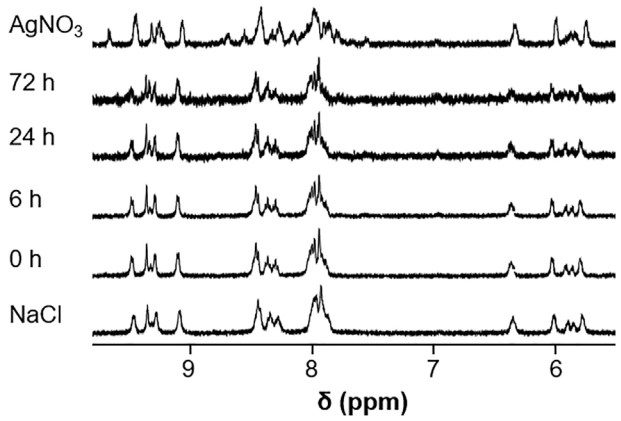

FIGURE 6 | ^{1}H NMR spectra of complex **2f** recorded in 10% DMSO-d_6/D_2O over a period of 72 h as well as after addition of $AgNO_3$ (2 equiv.) or NaCl (100 mM).

ligands coordinated to both Ru and Os) and **2d** (with Cp* ligands coordinated to both Rh and Ir), the metal centers were statistically distributed between the two positions in the crystal lattice; hence, it was not possible to distinguish between the two M(cym) or M(Cp*) moieties in the molecular structures. In contrast, in the structure of **2e**, the Ru and Ir centers could be unambiguously distinguished based on their different π-bound ligands, *i.e.*, cym and Cp*, respectively. For **2a** and **2d**, two independent molecules with *R*,*R* and *S*,*S* configurations at the metal centers were found in the unit cell, whereas in **2e** the two molecules had *R*,*S* and *S*,*R* configurations. For **2d** and **2e** the metal centers were arranged on opposite faces of the ligand whereas in **2a** the M(cym) moieties were found on the same face of the phenylene spacer (**Table 1**). In contrast to **2e**, the statistical distribution of the metal centers in **2a** and **2d** over the two sites, makes it impossible to determine accurately the M–donor atom bond lengths (**Table 1**).

Imines can hydrolyze in aqueous solution into the respective amine and aldehyde building blocks, and metal complexes may undergo ligand exchange reactions, especially in the presence of coordinating solvents like DMSO which is often used for the preparation of stock solutions for biological assays. Therefore, the stabilities of the representative complexes Os-Rh **2c** and Os-Ir **2f** were analyzed by ^{1}H NMR spectroscopy over a 72 h time period in DMSO-d_6 and 10% DMSO-d_6/D_2O. When **2c** was dissolved in DMSO-d_6, a second set of peaks appeared over a 72 h period suggesting coordination of DMSO to the Os center (**Supplementary Figure S21**). In the case of the Os-Ir compound **2f**, minor changes were observed, but these were not as pronounced as those observed for **2c** (**Supplementary Figure S22**). Interestingly, for the Cp* signals in the spectra of both compounds, we observed changes in the aliphatic region which require further investigations (Banerjee et al., 2018; Lee B. Y. T. et al., 2021; Lee B. et al., 2021). In 10% DMSO-d_6/D_2O, the spectra of **2f** changed over time which was suppressed by the addition of 100 mM NaCl, to approximate the standard chloride concentration in blood. In contrast, treatment with $AgNO_3$ resulted in precipitation of AgCl and significant alteration of the spectra, most likely owing to the formation of the aqua complex after abstraction of the chlorido ligand (**Figure 6**). An analogous pattern was observed in the case of **2c**, with the addition of $AgNO_3$ causing a precipitate of AgCl and a noticeable change in the shifts of the aromatic protons (**Supplementary Figure S23**). Note that in both experiments, precipitation occurred over the 72 h time period which resulted in spectra with lower signal-to-noise ratios which made the interpretation of the spectra more difficult.

All complexes were investigated for their cytotoxic activity in HCT116 (human colon cancer cell line), SW480 (human colon adenocarcinoma cell line), NCI-H460 (human non-small-cell lung cancer cell line) and SiHa (human cervical cancer cell line) cancer cell lines with the sulforhodamine B assay. Compounds that gave mean growth inhibitory concentrations (IC_{50}) > 100 μM were deemed to be inactive in the respective cell line. The IC_{50} values obtained for each complex have been summarized in **Table 2** and compared to the bidentate

TABLE 1 | Key bond lengths (Å) in the molecular structures of **2a**, **2d** and **2e**.

Bonds/bond lengths (Å)	2a		2d		2e	
	M1	M2	M1	M2	Ru	Ir
M–Cl	2.4008 (11)	2.3852 (13)	2.4052 (9)	2.4138 (8)	2.3738 (8)	2.3938 (8)
M–N	2.087 (4)	2.104 (4)	2.098 (3)	2.116 (3)	2.080 (3)	2.083 (3)
M–N	2.090 (4)	2.100 (4)	2.097 (3)	2.101 (3)	2.088 (3)	2.086 (3)

TABLE 2 | IC_{50} values (μM) complexes **2a**–**2f** in HCT116, NCI-H460, SiHa and SW480 cancer cell lines expressed as mean ± standard error (n = 3), in comparison to ligand **2** and the homodimetallic analogs $\mathbf{Ru}_2$, $\mathbf{Os}_2$, $\mathbf{Rh}_2$ and $\mathbf{Ir}_2$ (Steel et al., 2021).

Compound	IC_{50} value/μM			
	HCT116	NCI-H460	SiHa	SW480
2	55 ± 20	57 ± 6	88 ± 4	>100
$\mathbf{Ru}_2$	>100	>100	>100	>100
$\mathbf{Os}_2$	>100	>100	>100	>100
$\mathbf{Rh}_2$	70 ± 29	61 ± 13	70 ± 1	73 ± 4
$\mathbf{Ir}_2$	>100	>100	>100	>100
2a	>100	>100	>100	>100
2b	>100	>100	>100	>100
2c	>100	56 ± 12	77 ± 10	45 ± 9
2d	>100	>100	>100	>100
2e	>100	>100	>100	>100
2f	>100	>100	>100	>100

pyridyl-imine-based ligand **2** and the analogous homodimetallic complexes in the same cell lines and under the same conditions (Steel et al., 2021). Ligand **2** demonstrated only very moderate activity in HCT116, NCI-H460 and SiHa cells, while it was inactive in SW480. The formation of coordination compounds of **2** unfortunately did not significantly alter the overall picture, and only for Os-Rh compound **2c** IC_{50} values could be determined, which only showed moderate cytotoxicity. This reflects to a large extent the observations we made for the analogous homodiatomic complexes $\mathbf{Ru}_2$, $\mathbf{Os}_2$, $\mathbf{Rh}_2$ and $\mathbf{Ir}_2$ (Steel et al., 2021). While we and others have reported significant improvements in terms of cytotoxic effects when two or more metal centers are linked in a single molecule (Mendoza-Ferri et al., 2009), it is apparent that the incorporation of multiple metal centers in a single molecule does not necessarily result in high antiproliferative activity. The biological effect is significantly influenced by the ligand system used. This may in part be because of the structure of the ligand but may also be related to the stability of the formed complexes, with possibly even the ligands being the cytotoxic species upon cleavage of the metal centers from the coordinating motif. In any case, cellular accumulation of the active species is a prerequisite to observe biological activity which may be the reason for the low activity of this compound type (Jakupec et al., 2005). However, the low antiproliferative activity of the investigated complexes does not warrant further biological investigations.

3 CONCLUSION

In an attempt to improve the anticancer activity of organometallic anticancer agents, we designed and prepared heterodimetallic compounds based on a ditopic symmetric ligand. The synthetic strategy was developed by taking into consideration the labilities of the intermediate complexes to facilitate the isolation of the target heterodimetallic compounds in pure form. ^{1}H NMR spectroscopy in acetone-d_6 enabled the ligand components coordinated to the respective metal center to be distinguished, while ESI-MS confirmed the formation of the target compounds. Single crystal X-ray diffraction analysis showed statistical distribution of the metal centers in the heterometallic Ru/Os(cym) and Rh/Ir(Cp*) compounds **2a** and **2d**, while in case of complex **2e** the Ru(cym) and Ir(Cp*) moieties were easily distinguishable based on the π-bound ligand. Compounds **2c** and **2f** were investigated for stability in solution and both were found to undergo ligand exchange reactions, although at different rates. In assays to investigate antiproliferative activity, only **2c** showed very moderate potency. While the antiproliferative activity of the current complexes was only modest, the robust, facile and modular nature of the method to form these heterodimetallic compounds means that a wide range of systems could be synthesized and examined for biological activity. Furthermore, this method to heterodimetallic complexes may also find applications in the development of new catalysts (Mata et al., 2014; Gaston et al., 2021; Patra and Maity, 2021).

4 EXPERIMENTAL SECTION

4.1 Materials and Methods

All air and moisture-sensitive reactions were carried out under a nitrogen (N_2) atmosphere, and light sensitive reactions were protected from photolytic degradation by covering the apparatus in aluminum foil. Chemicals and solvents purchased from commercial suppliers were used without further purification. Solvents were dried prior to use when necessary. Solvents were evaporated under reduced pressure using a rotary evaporator. The precursor complexes $[Ru(cym)Cl_2]_2$ **a** (Bennett and Smith, 1974), $[Rh(Cp^*)Cl_2]_2$ **b** (Vogt et al., 2005; Nejman et al., 2015), $[Ir(Cp^*)Cl_2]_2$ **c** (Vogt et al., 2005; Jakoobi et al., 2017) and $[Os(cym)Cl_2]_2$ **d** (Peacock et al., 2007) were prepared according to literature procedures.

1D [^{1}H, and ^{13}C{^{1}H} DEPT-Q, ^{31}P{^{1}H}] and 2D (^{1}H-^{1}H COSY, ^{1}H-^{1}H NOESY, ^{1}H-^{13}C HSQC, ^{1}H-^{13}C HMBC) NMR spectra were recorded on Bruker DRX 400 MHz NMR spectrometers at 25 °C. The measurement frequencies for ^{1}H, ^{13}C{^{1}H}, and ^{31}P{^{1}H} NMR spectra were 399.89, 100.55 and 161.85 MHz, respectively. Deuterated chloroform, acetone-d_6, D_2O, and DMSO-d_6 were used as NMR solvents and the chemical shifts are reported relative to the residual solvent peaks. The mass spectra were recorded on a Bruker micrOTOF-Q II ESI-MS in positive ion mode. X-ray diffraction measurements of single crystals were conducted on a Rigaku Oxford Diffraction XtaLABSynergy-S single-crystal diffractometer with a PILATUS 200 K hybrid pixel array detector using Cu Kα radiation (λ = 1.54184 Å). The structure solution and refinements were performed with the SHELXS-97, SHELXL-2016 (Sheldrick, 2008) and Olex2 program packages (Dolomanov et al., 2009; Bourhis et al., 2015). Molecular structures were visualized using Mercury 4.0.0. Elemental analyses were carried out on the vario EL cube CHNOS Elemental analyzer at the University of Auckland for Ru, Rh,

and Ir complexes, and at the Campbell Microanalytical Laboratory, the University of Otago for Os complexes.

4.2 Syntheses

4.2.1 General Procedure for the Synthesis of Mononuclear Complexes 1a, 1c and 1d

Pyridyl-imine ligand **1** (1.0 eq) was added to a solution of dimeric precursor **a**, **c** or **d** (0.5 eq) in DCM:MeOH (15 ml, 1:1) and stirred at r. t. for 4 h. The solvent was then removed under reduced pressure. A solution of ammonium hexafluorophosphate (NH_4PF_6, 20 eq) in MeOH (20 ml) was added to a solution of the crude product in MeOH (20 ml) and the resulting mixture was stirred for 1 h. The solution was concentrated under reduced pressure and diethyl ether was added. The resulting precipitate was collected by filtration, washed with cold MeOH and dried. The crude product was dissolved in DCM (80 ml), filtered and the solvent was removed from the filtrate under reduced pressure to yield the products (**Figure 7** for the NMR numbering scheme) after drying the residue *in vacuo*.

[Chlorido(η^6-p-cymene)(4-((pyridine-2-ylmethylene)amino) aniline)ruthenium(II)] hexafluorophosphate **1a**.

1 (161 mg, 0.10 mmol), $[Ru(cym)Cl_2]_2$ **a** (250 mg, 0.05 mmol) and NH_4PF_6 (1.33 g, 1.02 mmol) to afford **1a** as a dark red powder (461 mg, 92%). m. p.: 104.8–118.2°C (decomposition). ^{1}H NMR (acetone-d_6): δ 9.55 (d, ^3J = 2 Hz, 1H, H-1), 8.73 (s, 1H, H-5), 8.32–8.24 (m, 2H, H-2,3), 7.84–7.79 (m, 1H, H-4), 7.69–7.64 (m, 2H, H-6), 6.87–6.81 (m, 2H, H-7), 6.11 (d, ^3J = 3 Hz, 1H, H-11), 5.77 (d, ^3J = 3 Hz, 1H, H-12), 5.72 (d, ^3J = 3 Hz, 1H, H-11), 5.66 (d, ^3J = 3 Hz, 1H, H-12), 5.45 (s, 2H, H-8), 2.68 (sept, ^3J = 7 Hz, 1H, H-10), 2.30 (s, 3H, H-13), 1.15–1.07 ppm (m, 6H, H-9). ^{13}C{^{1}H} DEPT-Q (acetone-d_6): δ 162.6 (C-5), 156.6 (C-1), 156.4 (C-4a), 151.9 (C-7a), 142.6 (C-5a), 140.6 (C-2,3), 129.6 (C-2,3), 128.9 (C-4), 125.2 (C-6), 114.6 (C-7), 106.8 (C-13), 104.8 (C-10), 87.9 (C-12), 87.3 (C-12), 86.7 (C-11), 85.9 (C-11), 31.9 (C-14), 22.2 (C-15), 18.7 ppm (C-9). ^{31}P{^{1}H} NMR (acetone-d_6): δ –144.29 ppm (sept, ^2J = 711 Hz, PF_6^-). MS (ESI$^+$): *m/z* 468.0788 $[M - PF_6]^+$ (m_{calc} = 468.0775).

[Chlorido(η^5-pentamethylcyclopentadienyl)(4-((pyridine-2-ylmethylene)amino)aniline)rhodium(III)] hexafluorophosphate **1b.**

The synthesis was performed according to the general procedure using **1** (128 mg, 0.65 mmol), $[Rh(Cp^*)Cl_2]_2$ **b** (201 mg, 0.32 mmol), and NH_4PF_6 (1.1 g, 6.5 mmol) to afford **1b** as a bright orange powder (335 mg, 84%). m. p.: 147 °C (clear point). ^{1}H NMR (DMSO-d_6): δ 8.98 (d, ^3J = 6 Hz, 1H, H-1), 8.76 (d, ^3J = 2 Hz, 1H, H-5), 8.31 (td, ^3J = 8 Hz, ^4J = 2 Hz, 1H, H-3), 8.20 (d, ^3J = 8 Hz, 1H, H-4), 7.91–7.86 (m, 1H, H-2), 7.49–7.43 (m, 2H, H-6), 6.72–6.70 (m, 2H, H-7), 5.79 (s, 2H, H-8), 1.45 ppm (s, 15H, H9). ^{13}C{^{1}H} DEPT-Q (DMSO-d_6): δ 162.3 (C-5), 154.4 (C-4a), 152.6 (C-1), 150.6 (C-5a), 140.3 (C-3), 137.2 (C-7a), 128.9 (C-2), 128.6 (C-4), 124.1 (C-6), 113.2 (C-7), 97.0 (C-9a), 8.3 ppm (C-9). ^{31}P{^{1}H} NMR (DMSO-d_6): δ –144.7 ppm (sept, ^2J = 711 Hz, PF_6^-). MS (ESI$^+$): *m/z* 470.0899 $[M - PF_6]^+$ (m_{calc} = 470.0870).

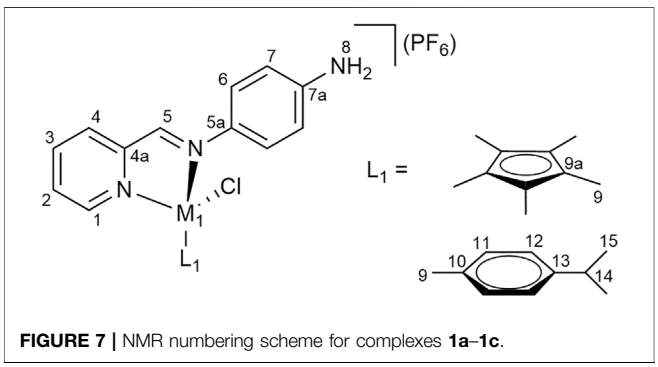

FIGURE 7 | NMR numbering scheme for complexes **1a**–**1c**.

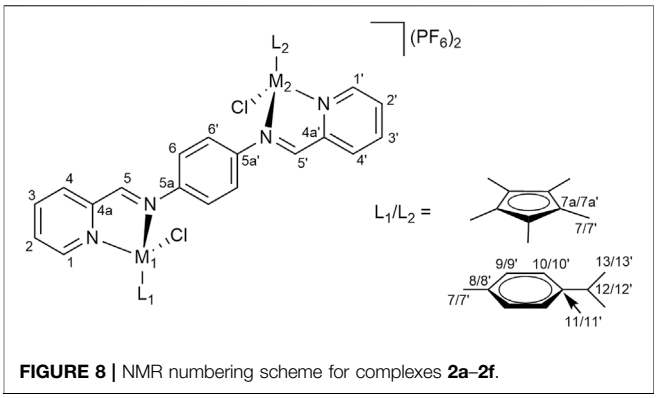

FIGURE 8 | NMR numbering scheme for complexes **2a**–**2f**.

[Chlorido(η^5-pentamethylcyclopentadienyl)(4-((pyridine-2-ylmethylene)amino)aniline)iridium(III)] hexafluorophosphate **1c.**

The synthesis was performed according to the general procedure using **1** (282 mg, 1.40 mmol), $[Ir(Cp^*)Cl_2]_2$ **c** (569 mg, 0.71 mmol), and NH_4PF_6 (3.5 g, 29 mmol) to afford **1c** as a dark orange powder (652 mg, 82%). m. p.: 176°C (clear point). ^{1}H NMR (DMSO-d_6): δ 9.14 (s, 1H, H-5), 8.97 (d, ^3J = 6 Hz, 1H, H-1), 8.33–8.25 (m, 2H, H-3/4), 7.89–7.83 (m, 1H, H-2), 7.41 (d, ^3J = 9 Hz, 2H, H-6), 6.68 (d, ^3J = 9 Hz, 2H, H-7), 5.80 (s, 2H, H-8), 1.44 ppm (s, 15H, H9). ^{13}C{^{1}H} DEPT-Q (DMSO-d_6): δ 163.8 (C-5), 156.0 (C-4a), 152.1 (C-1), 150.8 (C-5a), 140.5 (C-3/4), 137.6 (C-7a), 129.5 (C-2), 128.7 (C-3/4), 124.2 (C-6), 113.1 (C-7), 89.6 (C-9a), 8.0 ppm (C-9). ^{31}P{^{1}H} NMR (DMSO-d_6): δ –144.7 ppm (sept, ^2J = 711 Hz, PF_6^-). MS (ESI$^+$): *m/z* 560.1440 $[M - PF_6]^+$ (m_{calc} = 560.1444).

4.2.2 General Procedure for the Syntheses of Heterodimetallic Complexes 2a–2f

2-Pyridine carboxaldehyde (1 eq) was added to a solution of precursor complexes **1a**–**1c** (1 eq) in DCM:MeOH (30 ml, 1:1) and stirred at r. t. overnight. Dimeric precursor **a**, **b** or **d** (0.5 eq) was added and the resulting mixture was stirred for *ca.* 48 h. The solvent was removed under reduced pressure. A solution of NH_4PF_6 (20 eq) in MeOH (20 ml) was added to the solution of the crude product in MeOH (20 ml) and the resulting mixture was stirred for 1 h. The solution was concentrated under reduced pressure and diethyl ether was added. The precipitate was filtered, washed with cold MeOH and dried. The crude product was dissolved in acetone (40 ml), filtered and the solvent was removed from the filtrate under reduced pressure, yielding pure complexes (**Figure 8** for the NMR numbering scheme) after drying the residue *in vacuo*.

[Chlorido(η^6-p-cymene)osmium(II)](N,N'-(1,4-phenylene)(bis(1-(pyridin-2-yl)(methanimine)-κ^2N,N')[chlorido(η^6-p-cymene)ruthenium(II)] hexafluorophosphate **2a**.

The synthesis was performed according to the general procedure using **1a** (240 mg, 0.4 mmol), 2-pyridine carboxaldehyde (37 µL, 0.39 mmol), $[Os(cym)Cl_2]_2$ (158 mg, 0.20 mmol) and NH_4PF_6 (1.30 g, 8.0 mmol) to afford **2a** as a dark red-brown powder (397 mg, 84%). m. p.: 161.2–173.5°C (decomp.). ^{1}H NMR (acetone-d_6): δ 9.71 (d, ^3J = 2 Hz, 1H, H-1), 9.66 (d, ^3J = 3 Hz, 1H, H-1'), 9.46 (s, 1H, H-5'), 9.06 (s, 1H, H-5), 8.60–8.51 (m, 1H, H-3'), 8.48–8.36 (m, 3H, H-3,4', 4), 8.23–8.18 (m, 2H, H-6), 8.15–8.10 (m, 2H, H-6'), 8.00–7.91 (m, 2H, H-2,2'), 6.47 (d, ^3J = 4 Hz, 1H, H-9'), 6.19 (d, ^3J = 4 Hz, 1H, H-9), 6.10–6.02 (m, 2H, H-9'/10'), 5.91–5.83 (m, 3H, H-9, 10', 10), 5.71 (dd, ^3J = 8 Hz, ^4J = 3 Hz, 1H, H-10), 2.78 (m, 1H, H-12), 2.64 (sept, ^3J = 7 Hz 1H, H-12'), 2.40 (d, ^3J = 3 Hz, 3H, H-7), 2.33 (d, ^3J = 3 Hz, 3H, H-7'), 1.18–1.12 (m, 6H, H-13), 1.11–1.06 ppm (m, 6H, H-13'). ^{13}C{^{1}H} DEPT-Q (acetone-d_6): δ 170.0 (C-5'), 169.1 (C-5), 157.1 (C-1), 156.7 (C-1'), 155.8 (C-4a'), 154.2 (C-5a'), 154.0 (C-5a), 153.9 (C-4a), 141.2 (C-4,4'), 141.0 (C-4,4'), 131.5 (C-3), 131.3 (C-3'), 131.1 (C-2'), 130.2 (C-2), 125.4 (C-6'), 124.9 (C-6), 107.9 (C-11), 104.9 (C-8), 99.6 (C-11'), 98.8 (C-8'), 87.8 (C-9), 86.8 (C-9,10), 86.4 (C-10), 79.7 (C-9'), 79.1 (C-9'/10'), 77.3 (C-9'/10'), 76.9 (C-10'), 32.2 (C-12), 32.0 (C-12'), 22.6 (C-13'), 22.2 (C-13), 18.9 ppm (C-7,7'). ^{31}P{^{1}H} NMR (acetone-d_6): δ –144.37 ppm (sept, ^2J = 707 Hz, PF_6^-). MS (ESI$^+$): *m/z* 459.0721 $[M - 2PF_6]^{2+}$ (m_{calc} = 459.0723). EA calculated for $C_{38}H_{42}Cl_2F_{12}N_4P_2RuOs{\cdot}0.67NH_4PF_6$: C 34.69%, H 3.42%, N 4.97%. Found: C 35.03%, H 3.50%, N 5.07%.

[Chlorido(η^5-pentamethylcyclopentadienyl)rhodium(III)](N,N'-(1,4-phenylene)(bis(1-(pyridin-2-yl)(methanimine)-κ^2N,N')[chlorido(η^6-p-cymene)ruthenium(II)] hexafluorophosphate **2b**.

The synthesis was performed according to the general procedure using **1b** (165 mg, 0.27 mmol), 2-pyridine carboxaldehyde (26 µL, 0.27 mmol), $[Ru(cym)Cl_2]_2$ (82 mg, 0.14 mmol) and NH_4PF_6 (872 mg, 5.35 mmol) to afford **2b** as a yellow powder (152 mg, 51%). m. p.: 141°C (clear point). ^{1}H NMR (acetone-d_6): δ 9.69 (d, ^3J = 6 Hz, 1H, H-1'), 9.27–9.23 (m, 1H, H-1), 9.10–9.04 (m, 2H, H-5/5'), 8.49–8.37 (m, 4H, H-3/3'/4/4'), 8.25–8.18 (m, 1H, H-6'), 8.14–8.05 (m, 3H, H-2/6), 7.98–7.93 (m, 1H, H-2'), 6.21–6.16 (m, 1H, H-9'), 5.89–5.69 (m, 3H, H-8'/9'), 5.70 (d, ^3J = 6 Hz, 1H, H-8'), 2.74 (m, 1H, H-10'), 2.34–2.30 (m, 3H, H-7'), 1.69–1.63 (m, 15H, H-7), 1.20–1.12 ppm (m, 6H, H-11'). ^{13}C{^{1}H} DEPT-Q (acetone-d_6): δ 169.1 (C-5/5'), 157.0 (C-1'), 153.9 (C-1), 153.7 (C-4a/4a'/5a), 150.7 (C-4a/4a'), 150.6 (C-5a'), 141.6 (C-3/3'), 141.0 (C-3/3'), 131.5 (C-4/4'), 131.4 (C-4/4'), 131.2 (C-2), 130.2 (C-2'), 125.1 (C-6), 125.0 (C-6'), 107.8 (C-11'), 105.0 (C-8'), 98.7 (C-7a), 87.7–86.2 (C-9'/10'), 32.0 (C-12'), 22.3 (C-12'), 19.0 (C-7'), 9.0 ppm (C-7). ^{31}P{^{1}H} NMR (acetone-d_6): δ –144.3 ppm (sept, ^2J = 708 Hz, PF_6^-). MS (ESI$^+$): *m/z* 470.0870 $[M - 2PF_6 - C_6NH_5 - RuCl(p\text{-cym})]^+$ (m_{calc} = 470.0870). EA calculated for $C_{38}H_{43}Cl_2F_{12}RhN_4P_2Ru{\cdot}0.2NH_4PF_6$: C 39.57%, H 3.84%, N 5.10%. Found: C 39.67%, H 4.20%, N 4.80%.

[Chlorido(η^6-p-cymene)osmium(II)](N,N'-(1,4-phenylene)(bis(1-(pyridin-2-yl)(methanimine)-κ^2N,N')[chlorido(η^5-pentamethylcyclopentadienyl)rhodium(III)] hexafluorophosphate **2c.**

The synthesis was performed according to the general procedure using **1b** (153 mg, 0.25 mmol), 2-pyridine carboxaldehyde (24 µL, 0.25 mmol), $[Os(cym)Cl_2]_2$ (98 mg, 0.13 mmol) and NH_4PF_6 (808 mg, 4.96 mmol) to afford **2c** as an orange powder (127 mg, 42%). m. p.: 154°C (clear point). ^{1}H NMR (acetone-d_6): δ 9.64 (d, ^3J = 6 Hz, 1H, H-1'), 9.50 (s, 1H, H-5'), 9.26 (d, ^3J = 6 Hz, 1H, H-1), 9.06 (m, 1H, 1H, H-5), 8.55 (m, 1H, H-4'), 8.47–8.43 (m, 2H, H-3/4), 8.37 (m, 1H, H-3'), 8.16–8.07 (m, 5H, H-2/6/6'), 7.93–7.89 (m, 1H, H-2'), 6.49–6.45 (m, 1H, H-8'), 6.09–5.98 (m, 2H, H-8'/9'), 5.92–5.84 (m, 1H, H-9'), 2.64 (sept, ^3J = 7 Hz, 1H, H-10'), 2.41–2.37 (m, 3H, H-7'), 1.68–1.64 (m, 15H, H-7), 1.27–1.06 ppm (m, 6H, H-11'). ^{13}C{^{1}H} DEPT-Q (acetone-d_6): δ 170.0 (C-5'), 169.2 (C-5), 157.2 (C-4a'), 156.7 (C-1'), 153.9 (C-1), 153.7 (C-5a/5a'), 150.9 (C-5a/5a'), 141.6 (C-3), 141.1 (C-3'), 131.4 (C-4), 131.3 (C-4') 131.2 (C-2), 131.1 (C-2'), 125.5 (C-6/6'), 124.9 (C-6/6'), 99.5 (C-11'), 99.3 (C-8'), 98.6 (C-7a), 79.6–76.7 (C-9'/10'), 32.2 (C-12'), 22.6 (C-13'), 18.9 (C-7'), 9.0 ppm (C-7). ^{31}P{^{1}H} NMR (acetone-d_6): δ –144.3 ppm (sept, ^2J = 708 Hz, PF_6^-). MS (ESI$^+$): *m/z* 470.0817 $[M - 2PF_6 - C_6NH_5 - OsCl(p\text{-cym})]^+$ (m_{calc} = 470.0870). EA calculated for $C_{38}H_{43}Cl_2F_{12}RhN_4P_2Os$: C 37.73%, H 3.58%, N 4.63%. Found: C 37.77%, H 3.39%, N 4.44%.

[Chlorido(η^5-pentamethylcyclopentadienyl)iridium(III)](N,N'-(1,4-phenylene)(bis(1-(pyridin-2-yl)(methanimine)-κ^2N,N')[chlorido(η^5-pentamethylcyclopentadienyl)rhodium(III)] hexafluorophosphate **2d.**

The synthesis was performed according to the general procedure using **1c** (174 mg, 0.25 mmol), 2-pyridine carboxaldehyde (24 µL, 0.25 mmol), $[Rh(Cp^*)Cl_2]_2$ (76 mg, 0.13 mmol) and NH_4PF_6 (806 mg, 5.0 mmol) to afford **2d** as a dark yellow powder (170 mg, 58%). Single crystals suitable for X-ray diffraction analysis were grown by slow diffusion of toluene into a saturated solution of the complex in acetonitrile. m. p.: 135 °C (clear point). ^{1}H NMR (acetone-d_6): δ 9.53–9.50 (m, 1H, H-5), 9.27–9.23 (m, 2H, H-1/1'), 9.10 (dd, ^3J = 6 Hz, ^4J = 3 Hz, 1H, H-5'), 8.59–8.55 (m, 1H, H-4), 8.49–8.41 (m, 3H, H-3/3'/4'), 8.16–8.05 (m, 6H, H-2/2'/6/6'), 1.66–1.65 (m, 15H, H-7') 1.64–1.63 ppm (m, 15H, H-7). ^{13}C{^{1}H} DEPT-Q (acetone-d_6): δ 170.6 (C-5), 169.3 (C-5'), 153.8 (C-1/1'), 153.4 (C-1/1'), 150.7 (C-4a), 150.6 (C-4a'), 141.7 (C-4/4'), 141.5 (C-3/3'), 131.8 (C-2/2'), 131.4 (C-2/2'), 131.3 (C-4') 131.2 (C-4), 125.2 (C-6/6'), 124.9 (C-6/6'), 98.7 (C-7a'), 91.4 (C-7a), 9.0 (C-7'), 8.8 ppm (C-7). ^{31}P{^{1}H} NMR (acetone-d_6): δ –144.3 ppm (sept, ^2J = 707 Hz, PF_6^-). MS (ESI$^+$): *m/z* 461.0794 $[M - 2PF_6]^{2+}$ (m_{calc} = 461.0814). 461.0794. EA calculated for $C_{38}H_{44}Cl_2F_{12}IrN_4P_2Rh{\cdot}0.7H_2O$: C 37.24%, H 3.74%, N 4.57%. Found: C 36.84%, H 4.11%, N 4.39%.

[Chlorido(η^5-pentamethylcyclopentadienyl)iridium(III)](N,N'-(1,4-phenylene)(bis(1-(pyridin-2-yl)(methanimine)-κ^2N,N')[chlorido(η^6-p-cymene)ruthenium(II)] hexafluorophosphate **2e**.

The synthesis was performed according to the general procedure using **1c** (175 mg, 0.25 mmol), 2-pyridine carboxaldehyde (24 µL, 0.25 mmol), $[Ru(cym)Cl_2]_2$ (76 mg, 0.13 mmol) and NH_4PF_6

(808 mg, 5.0 mmol) to afford **2e** as a dark brown powder (151 mg, 50%). Single crystals suitable for X-ray diffraction analysis were grown by slow diffusion of toluene into a saturated solution of the complex in acetonitrile. m. p.: 169°C (clear point). ^{1}H NMR (acetone-d_6): δ 9.68 (d, ^3J = 6 Hz, 1H, H-1'), 9.48 (s, 1H, H-5), 9.25 (d, ^3J = 6 Hz, 1H, H-1), 9.08 (s, 1H, H-5'), 8.54–8.45 (m, 1H, H-4), 8.46–8.37 (m, 3H, H-3/3'/4'), 8.25–8.18 (m, 2H, H-6') 8.10–8.04 (m, 3H, H-2/6), 7.97–7.92 (m, 1H, H-2') 6.21–6.15 (m, 1H, H-9'), 5.87–5.73 (m, 2H, H-8'/9'), 5.69 (d ^3J = 6 Hz, 1H, H-8'), 2.75 (m, 1H, H-10'), 2.32 (s, 3H, H-7'), 1.65–1.62 (m, 15H, H-7), 1.19–1.13 ppm (m, 6H, H-11'). ^{13}C{^{1}H} DEPT-Q (acetone-d_6): δ 170.5 (C-5), 169.2 (C-5'), 157.0 (C-1'), 156.5 (C-4a'), 155.7 (C-4a), 153.9 (C-5a), 153.4 (C-1), 150.9 (C-5a'), 141.7 (C-3/3') 141.0 (C-3/3'), 131.8 (C-2), 131.5 (C-4), 131.3 (C-4'), 130.2 (C-2'), 125.1 (C-6'), 125.0 (C-6), 107.8 (C-11'), 105.1 (C-8'), 91.4 (C-7a), 87.8–86.2 (C-9'/10'), 32.0 (C-12'), 22.3 (C-13'), 18.9 (C-7'), 8.7 ppm (C-7). ^{31}P{^{1}H} NMR (acetone-d_6): δ −144.3 ppm (sept, ^2J = 708 Hz, PF_6^-). MS (ESI$^+$): *m/z* 460.0785 $[M - 2PF_6]^{2+}$ (m_{calc} = 460.0769). EA calculated for $C_{38}H_{43}Cl_2F_{12}IrN_4P_2Ru{\cdot}0.9H_2O$: C 37.22%, H 3.68%, N 4.57%. Found: C 36.87%, H 3.72%, N 4.95%.

[Chlorido(η^5-pentamethylcyclopentadienyl)iridium(III)](N,N'-(1,4-phenylene)(bis(1-(pyridin-2-yl)(methanimine)-κ^{2}N,N')[chlorido(η^6-p-cymene)osmium(II)] hexafluorophosphate **2f**.

The synthesis was performed according to the general procedure using **1c** (163 mg, 0.23 mmol), 2-pyridine carboxaldehyde (22 μL, 0.23 mmol), $[Os(cym)Cl_2]_2$ (91 mg, 0.12 mmol) and NH_4PF_6 (753 mg, 4.6 mmol) to afford **2f** as a dark red powder (201 mg, 67%). m. p.: 147°C (clear point). ^{1}H NMR acetone-d_6): δ 9.64 (d, ^3J = 6 Hz, 1H, H-1'), 9.49–9.47 (m, 2H, H-5/5'), 9.25 (d, ^3J = 6 Hz, 1H, H-1), 8.59–8.54 (m, 2H, H-4/4'), 8.44 (td, ^3J = 8 Hz, ^3J = 1 Hz, 1H, H-3), 8.38 (m, 1H, H-3'), 8.16–8.12 (m, 2H, H-6'), 8.11–8.04 (m, 3H, H-2/6), 7.94–7.89 (m, 1H, H-2'), 6.50–6.44 (m, 1H, H-9'), 6.08–5.98 (m, 2H, H-8'/9'), 5.87 (dd, ^3J = 20.6 Hz, ^4J = 5.8 Hz, 1H, H8'), 2.63 (sept, ^3J = 7 Hz, 1H, H-10'), 2.39 (d, ^3J = 7.2 Hz, 3H, H-7'), 1.67–1.62 (m, 15H, H-7), 1.12–1.07 ppm (m, 6H, H-11'). ^{13}C{^{1}H} DEPT-Q (acetone-d_6): δ 170.7 (C-5/5'), 170.1 (C-5/5'), 157.1 (C-4a'), 156.5 (C-4a) 156.7 (C-1'), 154.0 (C-5a), 153.4 (C-1), 151.0 (C-5a'), 141.7 (C-4), 141.1 (C-4'), 131.8 (C-2), 131.4 (C-3/3'), 131.1 (C-2'), 125.4 (C-6/6'), 125.15 (C-6/6'), 99.6 (C-11'), 99.4 (C-8'), 91.4 (C-7a), 79.6–76.7 (C-9'/10'), 32.2 (C-12'), 22.6 (C-13'), 19.0 (C-7'), 8.7 ppm (C-7). ^{31}P{^{1}H} NMR (acetone-d_6): δ −144.3 ppm (sept, ^2J = 708 Hz, PF_6^-). MS (ESI$^+$): *m/z* 505.1053 $[M - 2PF_6]^{2+}$ (m_{calc} = 505.1055). EA calculated for $C_{38}H_{43}Cl_2F_{12}IrN_4P_2Os{\cdot}0.6H_2O$: C 34.84%, H 3.41%, N 4.28%. Found: C 34.44%, H 3.29%, N 4.04%.

4.3 DMSO and Aqueous Stability Studies

Stability studies in DMSO were conducted for **2c** and **2f** by dissolving *ca.* 1 mg of the complex in DMSO-d_6 (*ca.* 0.5 ml). ^{1}H NMR spectra were recorded at t = 0, 2, 6, 24, 48, and 72 h.

The stability studies in aqueous solution were conducted by dissolving *ca.* 1 mg of **2c** or **2f** in DMSO-d_6 (0.05 ml) and diluting it with D_2O (0.45 ml) to form a 10% DMSO-d_6/D_2O solution. ^{1}H NMR spectra were recorded at t = 0, 2, 6, 24, 48, and 72 h. The compounds were investigated *via* the same procedure in a solution of 100 mM NaCl in D_2O (0.45 ml) added to a solution of *ca.* 1 mg of the complex in DMSO-d_6 (0.05 ml). In addition, a solution of the hydrolyzed product was prepared by the addition of $AgNO_3$ (2 eq) to a suspension of *ca.* 1 mg of the complex (1 eq) in 10% DMSO-d_6/D_2O. After vigorous shaking, the formed AgCl was removed by filtration and a ^{1}H NMR spectrum of the filtrate was recorded.

4.4 Cell Cytotoxicity Studies

The antiproliferative activity of compounds **2a**–**2f** was investigated in HCT116, SW480, SiHa and NCI-H460 cells as described elsewhere (Movassaghi et al., 2018). In brief, the cells were grown in α-MEM supplemented with 5% fetal calf serum at 37°C in a humidified incubator with 5% CO_2 after seeding them at 750 (HCT116, NCI-H460), 4,000 (SiHa) and 5,000 (SW480) cells per well in 96-well plates. The complexes were added to the plates in a series of 3-fold dilutions in 0.5% DMSO at the highest concentration for 72 h before the assay was terminated and the cells were stained with 0.4% sulforhodamine B (Sigma-Aldrich). The IC_{50} values were calculated with SigmaPlot 14.0 (Systat Software Inc.) using a three-parameter logistic sigmoidal dose-response curve between the calculated growth inhibition and the compound concentration. The presented IC_{50} values are the mean of at least three independent experiments, where 10 concentrations were tested in duplicate for each compound.

DATA AVAILABILITY STATEMENT

The original contributions presented in the study are included in the article/**Supplementary Material**, further inquiries can be directed to the corresponding author.

AUTHOR CONTRIBUTIONS

LG and TRS synthesized the compounds under supervision of MH and CH, TS refined the molecular structures, and LG and MR determined the cytotoxicity supervised by SJ. The project was conceptualized by LW, JC and CH, and the manuscript was drafted by LG and CH and finalized with input from all co-authors.

FUNDING

The project was funded through the Marsden Fund Council, managed by the Royal Society Te Apārangi. MH is supported by a Sir Charles Hercus Fellowship of the Health Research Council of New Zealand.

ACKNOWLEDGMENTS

We would like to thank the University of Auckland for Doctoral Scholarships to LG and TS and a Faculty Research Development Fund grant of the Faculty of Science to MH. We are grateful to Tanya Groutso for collecting the X-ray diffraction, and to Tony Chen and Mansa Nair for collecting the MS data. MR would like to thank Eva and Henry Frænkels Minde fond, Knud Højgaards

Fond, Dagmar Marshalls Fond, Carl og Ellen Hertz' legat til Dansk Læge-og Naturvidenskab, Viet-Jacobsen Fonden, Christian og Ottilia Brorsons Rejselegat for yngre videnskabsmænd—og kvinder, and Direktør Jacob Madsens og Hustru Olga Madsens Fond for financial support.

REFERENCES

Arango, D., Wilson, A. J., Shi, Q., Corner, G. A., Arañes, M. J., Nicholas, C., et al. (2004). Molecular Mechanisms of Action and Prediction of Response to Oxaliplatin in Colorectal Cancer Cells. *Br. J. Cancer.* 91, 1931–1946. doi:10.1038/sj.bjc.6602215

Banerjee, S., Soldevila-Barreda, J. J., Wolny, J. A., Wootton, C. A., Habtemariam, A., Romero-Canelón, I., et al. (2018). New Activation Mechanism for Half-Sandwich Organometallic Anticancer Complexes. *Chem. Sci.* 9, 3177–3185. doi:10.1039/c7sc05058e

Batchelor, L. K., Ortiz, D., and Dyson, P. J. (2019). Histidine Targeting Heterobimetallic Ruthenium(II)-Gold(I) Complexes. *Inorg. Chem.* 58, 2501–2513. doi:10.1021/acs.inorgchem.8b03069

Benjamin Garbutcheon-Singh, K., Grant, M., Harper, B., Krause-Heuer, A., Manohar, M., Orkey, N., et al. (2011). Transition Metal Based Anticancer Drugs. *Curr. Top. Med. Chem.* 11, 521–542. doi:10.2174/156802611794785226

Bennett, M. A., and Smith, A. K. (1974). Arene Ruthenium(II) Complexes Formed by Dehydrogenation of Cyclohexadienes With Ruthenium(III) Trichloride. *J. Chem. Soc. Dalton Trans.*, 233–241. doi:10.1039/dt9740000233

Bertrand, B., Doulain, P.-E., Goze, C., and Bodio, E. (2016). Development of Trackable Metal-Based Drugs: New Generation of Therapeutic Agents. *Dalton Trans.* 45, 13005–13011. doi:10.1039/c5dt04275e

Bertrand, B., Passador, K., Goze, C., Denat, F., Bodio, E., and Salmain, M. (2018). Metal-Based BODIPY Derivatives as Multimodal Tools for Life Sciences. *Coord. Chem. Rev.* 358, 108–124. doi:10.1016/j.ccr.2017.12.007

Boros, E., Dyson, P. J., and Gasser, G. (2020). Classification of Metal-Based Drugs According to Their Mechanisms of Action. *Chem.* 6, 41–60. doi:10.1016/j.chempr.2019.10.013

Bourhis, L. J., Dolomanov, O. V., Gildea, R. J., Howard, J. A. K., and Puschmann, H. (2015). The Anatomy of a Comprehensive Constrained, Restrained Refinement Program for the Modern Computing Environment -Olex2 dissected. *Acta Cryst. Sect. A.* 71, 59–75. doi:10.1107/s2053273314022207

Buccella, D., Lim, M. H., and Morrow, J. R. (2019). Metals in Biology: From Metallomics to Trafficking. *Inorg. Chem.* 58, 13505–13508. doi:10.1021/acs.inorgchem.9b02965

Burgoyne, A. R., Kaschula, C. H., Parker, M. I., and Smith, G. S. (2016). *In Vitro* Cytotoxicity of Half-Sandwich Platinum Group Metal Complexes of a Cationic Alkylated Phosphaadamantane Ligand. *Eur. J. Inorg. Chem.* 2016, 1267–1273. doi:10.1002/ejic.201501458

Curado, N., Giménez, N., Miachin, K., Aliaga-Lavrijsen, M., Cornejo, M. A., Jarzecki, A. A., et al. (2019). Preparation of Titanocene-Gold Compounds Based on Highly Active Gold(I)-*N*-Heterocyclic Carbene Anticancer Agents: Preliminary *In Vitro* Studies in Renal and Prostate Cancer Cell Lines. *ChemMedChem.* 14, 1086–1095. doi:10.1002/cmdc.201800796

Dolomanov, O. V., Bourhis, L. J., Gildea, R. J., Howard, J. A. K., and Puschmann, H. (2009). OLEX2: a Complete Structure Solution, Refinement and Analysis Program. *J. Appl. Cryst.* 42, 339–341. doi:10.1107/s0021889808042726

Gaston, A. J., Greindl, Z., Morrison, C. A., and Garden, J. A. (2021). Cooperative Heterometallic Catalysts for Lactide Ring-Opening Polymerization: Combining Aluminum With Divalent Metals. *Inorg. Chem.* 60, 2294–2303. doi:10.1021/acs.inorgchem.0c03145

Geldmacher, Y., Oleszak, M., and Sheldrick, W. S. (2012). Rhodium(III) and Iridium(III) Complexes as Anticancer Agents. *Inorg. Chim. Acta* 393, 84–102. doi:10.1016/j.ica.2012.06.046

Ghosh, A. C., Duboc, C., and Gennari, M. (2021). Synergy Between Metals for Small Molecule Activation: Enzymes and Bio-Inspired Complexes. *Coord. Chem. Rev.* 428, 213606. doi:10.1016/j.ccr.2020.213606

Gonchar, M. R., Matnurov, E. M., Burdina, T. A., Zava, O., Ridel, T., Milaeva, E. R., et al. (2020). Ruthenium(II)-Arene and Triruthenium-Carbonyl Cluster Complexes With New Water-Soluble Phopsphites Based on Glucose: Synthesis, Characterization and Antiproliferative Activity. *J. Organomet. Chem.* 919, 121312. doi:10.1016/j.jorganchem.2020.121312

Gorle, A. K., Haselhorst, T., Katner, S. J., Everest-Dass, A. V., Hampton, J. D., Peterson, E. J., et al. (2021). Conformational Modulation of Iduronic Acid-Containing Sulfated Glycosaminoglycans by a Polynuclear Platinum Compound and Implications for Development of Antimetastatic Platinum Drugs. *Angew. Chem.* 133, 3320–3326. doi:10.1002/ange.202013749

Gorle, A. K., Katner, S. J., Johnson, W. E., Lee, D. E., Daniel, A. G., Ginsburg, E. P., et al. (2018). Substitution-Inert Polynuclear Platinum Complexes as Metalloshielding Agents for Heparan Sulfate. *Chem. Eur. J.* 24, 6606–6616. doi:10.1002/chem.201706030

Haas, K. L., and Franz, K. J. (2009). Application of Metal Coordination Chemistry to Explore and Manipulate Cell Biology. *Chem. Rev.* 109, 4921–4960. doi:10.1021/cr900134a

Hartinger, C. G., Jakupec, M. A., Zorbas-Seifried, S., Groessl, M., Egger, A., Berger, W., et al. (2008). KP1019, A New Redox-Active Anticancer Agent - Preclinical Development and Results of a Clinical Phase I Study in Tumor Patients. *Chem. Biodiversity* 5, 2140–2155. doi:10.1002/cbdv.200890195

Heffeter, P., Böck, K., Atil, B., Reza Hoda, M. A., Körner, W., Bartel, C., et al. (2010). Intracellular Protein Binding Patterns of the Anticancer Ruthenium Drugs KP1019 and KP1339. *J. Biol. Inorg. Chem.* 15, 737–748. doi:10.1007/s00775-010-0642-1

Herry, B., Batchelor, L. K., Roufosse, B., Romano, D., Baumgartner, J., Borzova, M., et al. (2019). Heterobimetallic Ru(μ-dppm)Fe and Homobimetallic Ru(μ-dppm)Ru Complexes as Potential Anti-Cancer Agents. *J. Organomet. Chem.* 901, 120934. doi:10.1016/j.jorganchem.2019.120934

Jain, A. (2019). Multifunctional, Heterometallic Ruthenium-Platinum Complexes With Medicinal Applications. *Coord. Chem. Rev.* 401, 213067. doi:10.1016/j.ccr.2019.213067

Jakoobi, M., Halcovitch, N., Whitehead, G. F. S., and Sergeev, A. G. (2017). Selective Arene Cleavage by Direct Insertion of Iridium Into the Aromatic Ring. *Angew. Chem.* 129, 3314–3317. doi:10.1002/ange.201611409

Jakupec, M. A., Galanski, M., Arion, V. B., Hartinger, C. G., and Keppler, B. K. (2008). Antitumour Metal Compounds: More Than Theme and Variations. *Dalton Trans.*, 183–194. doi:10.1039/b712656p

Jakupec, M. A., Reisner, E., Eichinger, A., Pongratz, M., Arion, V. B., Galanski, M., et al. (2005). Redox-Active Antineoplastic Ruthenium Complexes With Indazole: Correlation of *In Vitro* Potency and Reduction Potential. *J. Med. Chem.* 48, 2831–2837. doi:10.1021/jm0490742

Johnstone, T. C., Park, G. Y., and Lippard, S. J. (2014). Understanding and Improving Platinum Anticancer Drugs-Pphenanthriplatin. *Anticancer Res.* 34, 471–476.

Kenny, R. G., and Marmion, C. J. (2019). Toward Multi-Targeted Platinum and Ruthenium Drugs-A New Paradigm in Cancer Drug Treatment Regimens? *Chem. Rev.* 119, 1058–1137. doi:10.1021/acs.chemrev.8b00271

Lee, B. Y. T., Phillips, A. D., Hanif, M., Tong, K. K. H., Söhnel, T., and Hartinger, C. G. (2021a). Heptadentate, Octadentate, or Even Nonadentate? Denticity in the Unexpected Formation of an All-Carbon Donor-Atom Ligand in Rh^{III}(Cp*)(Anthracenyl-NHC) Complexes. *Inorg. Chem.* 60, 8734–8741. doi:10.1021/acs.inorgchem.1c00711

Lee, B. Y. T., Sullivan, M. P., Yano, E., Tong, K. K. H., Hanif, M., Kawakubo-Yasukochi, T., et al. (2021b). Anthracenyl Functionalization of Half-Sandwich Carbene Complexes: *In Vitro* Anticancer Activity and Reactions With Biomolecules. *Inorg. Chem.* 60, 19, 14636–14644. doi:10.1021/acs.inorgchem.1c01675

Lisboa, L. S., Findlay, J. A., Wright, L. J., Hartinger, C. G., and Crowley, J. D. (2020). A Reduced-Symmetry Heterobimetallic $[PdPtL_4]^{4+}$ Cage: Assembly, Guest Binding, and Stimulus-Induced Switching. *Angew. Chem. Int. Ed.* 59, 11101–11107. doi:10.1002/anie.202003220

SUPPLEMENTARY MATERIAL

The Supplementary Material for this article can be found online at: https://www.frontiersin.org/articles/10.3389/fchem.2021.786367/full#supplementary-material

Lisboa, L. S., Riisom, M., Vasdev, R. A. S., Jamieson, S. M. F., Wright, L. J., Hartinger, C. G., et al. (2021). Cavity-Containing $[Fe_2L_3]^{4+}$ Helicates: An Examination of Host-Guest Chemistry and Cytotoxicity. *Front. Chem.* 9, 697684. doi:10.3389/fchem.2021.739785

Maillet, A., Yadav, S., Loo, Y. L., Sachaphibulkij, K., and Pervaiz, S. (2013). A Novel Osmium-Based Compound Targets the Mitochondria and Triggers ROS-Dependent Apoptosis in Colon Carcinoma. *Cell Death Dis.* 4, e653. doi:10.1038/cddis.2013.185

Manzotti, C., Pratesi, G., Menta, E., Di Domenico, R., Cavalletti, E., Fiebig, H. H., et al. (2000). BBR 3464: a Novel Triplatinum Complex, Exhibiting a Preclinical Profile of Antitumor Efficacy Different From Cisplatin. *Clin. Cancer Res.* 6, 2626–2634.

Mata, J. A., Hahn, F. E., and Peris, E. (2014). Heterometallic Complexes, Tandem Catalysis and Catalytic Cooperativity. *Chem. Sci.* 5, 1723–1732. doi:10.1039/c3sc53126k

Mendoza-Ferri, M.-G., Hartinger, C. G., Eichinger, R. E., Stolyarova, N., Severin, K., Jakupec, M. A., et al. (2008). Influence of the Spacer Length on the *In Vitro* Anticancer Activity of Dinuclear Ruthenium−Arene Compounds. *Organometallics* 27, 2405–2407. doi:10.1021/om800207t

Mendoza-Ferri, M. G., Hartinger, C. G., Mendoza, M. A., Groessl, M., Egger, A. E., Eichinger, R. E., et al. (2009). Transferring the Concept of Multinuclearity to Ruthenium Complexes for Improvement of Anticancer Activity. *J. Med. Chem.* 52, 916–925. doi:10.1021/jm8013234

Movassaghi, S., Singh, S., Mansur, A., Tong, K. K. H., Hanif, M., Holtkamp, H. U., et al. (2018). (Pyridin-2-yl)-NHC Organoruthenium Complexes: Antiproliferative Properties and Reactivity Toward Biomolecules. *Organometallics* 37, 1575–1584. doi:10.1021/acs.organomet.8b00153

Nazarov, A. A., Mendoza-Ferri, M.-G., Hanif, M., Keppler, B. K., Dyson, P. J., and Hartinger, C. G. (2018). Understanding the Interactions of Diruthenium Anticancer Agents With Amino Acids. *J. Biol. Inorg. Chem.* 23, 1159–1164. doi:10.1007/s00775-018-1597-x

Nejman, P. S., Morton-Fernandez, B., Moulding, D. J., Athukorala Arachchige, K. S., Cordes, D. B., Slawin, A. M. Z., et al. (2015). Structural Diversity of Bimetallic Rhodium and Iridium Half Sandwich Dithiolato Complexes. *Dalton Trans.* 44, 16758–16766. doi:10.1039/c5dt02542g

Nováková, O., Nazarov, A. A., Hartinger, C. G., Keppler, B. K., and Brabec, V. (2009). DNA Interactions of Dinuclear Ru^{II} Arene Antitumor Complexes in Cell-Free media. *Biochem. Pharmacol.* 77, 364–374. doi:10.1016/j.bcp.2008.10.021

Parveen, S., Arjmand, F., and Tabassum, S. (2019a). Development and Future Prospects of Selective Organometallic Compounds as Anticancer Drug Candidates Exhibiting Novel Modes of Action. *Eur. J. Med. Chem.* 175, 269–286. doi:10.1016/j.ejmech.2019.04.062

Parveen, S., Hanif, M., Leung, E., Tong, K. K. H., Yang, A., Astin, J., et al. (2019b). Anticancer Organorhodium and -iridium Complexes with Low Toxicity *In Vivo* but High Potency *In Vitro*: DNA Damage, Reactive Oxygen Species Formation, and Haemolytic Activity. *Chem. Commun.* 55, 12016–12019. doi:10.1039/c9cc03822a

Patra, S., and Maity, N. (2021). Recent Advances in (Hetero)Dimetallic Systems Towards Tandem Catalysis. *Coord. Chem. Rev.* 434, 213803. doi:10.1016/j.ccr.2021.213803

Payne, R., Govender, P., Therrien, B., Clavel, C. M., Dyson, P. J., and Smith, G. S. (2013). Neutral and Cationic Multinuclear Half-Sandwich Rhodium and Iridium Complexes Coordinated to Poly(propyleneimine) Dendritic Scaffolds: Synthesis and Cytotoxicity. *J. Organomet. Chem.* 729, 20–27. doi:10.1016/j.jorganchem.2013.01.009

Peacock, A. F. A., Habtemariam, A., Moggach, S. A., Prescimone, A., Parsons, S., and Sadler, P. J. (2007). Chloro Half-Sandwich Osmium(II) Complexes: Influence of Chelated N,N-ligands on Hydrolysis, Guanine Binding, and Cytotoxicity. *Inorg. Chem.* 46, 4049–4059. doi:10.1021/ic062350d

Redrado, M., Fernández-Moreira, V., and Gimeno, M. C. (2021). Theranostics Through the Synergistic Cooperation of Heterometallic Complexes. *ChemMedChem.* 16, 932–941. doi:10.1002/cmdc.202000833

Ruhayel, R. A., Langner, J. S., Oke, M.-J., Berners-Price, S. J., Zgani, I., and Farrell, N. P. (2012). Chimeric Platinum-Polyamines and DNA Binding. Kinetics of DNA Interstrand Cross-Link Formation by Dinuclear Platinum Complexes With Polyamine Linkers. *J. Am. Chem. Soc.* 134, 7135–7146. doi:10.1021/ja301397h

Sava, G., Zorzet, S., Turrin, C., Vita, F., Soranzo, M., Zabucchi, G., et al. (2003). Dual Action of NAMI-A in Inhibition of Solid Tumor Metastasis: Selective Targeting of Metastatic Cells and Binding to Collagen. *Clin. Cancer Res.* 9, 1898–1905.

Sheldrick, G. M. (2008). A Short History of SHELX. *Acta Cryst. Sect. A.* 64, 112–122. doi:10.1107/s0108767307043930

Simpson, P. V., Desai, N. M., Casari, I., Massi, M., and Falasca, M. (2019). Metal-Based Antitumor Compounds: beyond Cisplatin. *Future Med. Chem.* 11, 119–135. doi:10.4155/fmc-2018-0248

Steel, T. R., Tong, K. K. H., Söhnel, T., Jamieson, S. M. F., Wright, L. J., Crowley, J. D., et al. (2021). Homodinuclear Organometallics of Ditopic N,N-chelates: Synthesis, Reactivity and *In Vitro* Anticancer Activity. *Inorg. Chim. Acta* 518, 120220. doi:10.1016/j.ica.2020.120220

Tremlett, W. D. J., Goodman, D. M., Steel, T. R., Kumar, S., Wieczorek-Błauż, A., Walsh, F. P., et al. (2021). Design Concepts of Half-sandwich Organoruthenium Anticancer Agents Based on Bidentate Bioactive Ligands. *Coord. Chem. Rev.* 445, 213950. doi:10.1016/j.ccr.2021.213950

Vogt, M., Pons, V., and Heinekey, D. M. (2005). Synthesis and Characterization of a Dicationic Dihydrogen Complex of Iridium With a Bis-Carbene Ligand Set. *Organometallics* 24, 1832–1836. doi:10.1021/om049045p

Wodrich, M. D., and Hu, X. (2017). Natural Inspirations for Metal–Ligand Cooperative Catalysis. *Nat. Rev. Chem.* 2, 1–7. doi:10.1038/s41570-017-0099

Conflict of Interest: The authors declare that the research was conducted in the absence of any commercial or financial relationships that could be construed as a potential conflict of interest.

Publisher's Note: All claims expressed in this article are solely those of the authors and do not necessarily represent those of their affiliated organizations, or those of the publisher, the editors and the reviewers. Any product that may be evaluated in this article, or claim that may be made by its manufacturer, is not guaranteed or endorsed by the publisher.